Simultaneously Mitigating Near-Term Climate Change and Improving Human Health and Food Security

Drew Shindell *et al.*

Science **335**, 183 (2012);
DOI: 10.1126/science.1210026

Science (print ISSN 0036-8075; online ISSN 1095-9203) is published weekly, except the last week in December, by the American Association for the Advancement of Science, 1200 New York Avenue NW, Washington, DC 20005.

Simultaneously Mitigating Near-Term Climate Change and Improving Human Health and Food Security

Drew Shindell,[1]* Johan C. I. Kuylenstierna,[2] Elisabetta Vignati,[3] Rita van Dingenen,[3] Markus Amann,[4] Zbigniew Klimont,[4] Susan C. Anenberg,[5] Nicholas Muller,[6] Greet Janssens-Maenhout,[3] Frank Raes,[3] Joel Schwartz,[7] Greg Faluvegi,[1] Luca Pozzoli,[3]† Kaarle Kupiainen,[4] Lena Höglund-Isaksson,[4] Lisa Emberson,[2] David Streets,[8] V. Ramanathan,[9] Kevin Hicks,[2] N. T. Kim Oanh,[10] George Milly,[1] Martin Williams,[11] Volodymyr Demkine,[12] David Fowler[13]

Tropospheric ozone and black carbon (BC) contribute to both degraded air quality and global warming. We considered ~400 emission control measures to reduce these pollutants by using current technology and experience. We identified 14 measures targeting methane and BC emissions that reduce projected global mean warming ~0.5°C by 2050. This strategy avoids 0.7 to 4.7 million annual premature deaths from outdoor air pollution and increases annual crop yields by 30 to 135 million metric tons due to ozone reductions in 2030 and beyond. Benefits of methane emissions reductions are valued at $700 to $5000 per metric ton, which is well above typical marginal abatement costs (less than $250). The selected controls target different sources and influence climate on shorter time scales than those of carbon dioxide–reduction measures. Implementing both substantially reduces the risks of crossing the 2°C threshold.

Tropospheric ozone and black carbon (BC) are the only two agents known to cause both warming and degraded air quality. Although all emissions of BC or ozone precursors [including methane (CH_4)] degrade air quality, and studies document the climate effects of total anthropogenic BC and tropospheric ozone (*1*–*4*), published literature is inadequate to address many policy-relevant climate questions regarding these pollutants because emissions of ozone precursors have multiple cooling and warming effects, whereas BC is emitted along with other particles that cause cooling, making the net effects of real-world emissions changes obscure. Such information is needed, however, because multiple stakeholders are interested in mitigating climate change via control of non–carbon dioxide (CO_2)–forcing agents such as BC, including the G8 nations (L'Aquila Summit, 2009) and the Arctic Council (Nuuk Declaration, 2011). Here, we show that implementing specific practical emissions reductions chosen to maximize climate benefits would have important "win-win" benefits for near-term climate, human health, agriculture, and the cryosphere, with magnitudes that vary strongly across regions. We also quantify the monetized benefits due to health, agriculture, and global mean climate change per metric ton of CH_4 and for the BC measures as a whole and compare these with implementation costs.

Our analysis proceeded in steps. Initially, ~400 existing pollution control measures were screened with the International Institute for Applied Systems Analysis Greenhouse Gas and Air Pollution Interactions and Synergies (IIASA GAINS) model (*5*, *6*). The model estimated potential worldwide emissions reductions of particulate and gaseous species on the basis of available real-world data on reduction efficiencies of these measures where they have been applied already and examined the impact of full implementation everywhere by 2030. Their potential climate impact was assessed by using published global warming potential (GWP) values for each pollutant affected. All emissions control measures are assumed to improve air quality. We then selected measures that both mitigate warming and improve air quality, ranked by climate impact. If enhanced air quality had been paramount, the selected measures would be quite different [for example, measures primarily reducing sulfur dioxide (SO_2) emissions improve air quality but may increase warming]. The screening revealed that the top 14 measures realized nearly 90% of the maximum reduction in net GWP (table S1 and fig. S2). Seven measures target CH_4 emissions, covering coal mining, oil and gas production, long-distance gas transmission, municipal waste and landfills, wastewater, livestock manure, and rice paddies. The others target emissions from incomplete combustion and include technical measures (set "Tech"), covering diesel vehicles, clean-burning biomass stoves, brick kilns, and coke ovens, as well as primarily regulatory measures (set "Reg"), including banning agricultural waste burning, eliminating high-emitting vehicles, and providing modern cooking and heating. We refer to these seven as "BC measures," although in practice, we consider all co-emitted species (*7*).

We then developed future emissions scenarios to investigate the effects of the emissions control measures in comparison with both a reference and a potential low-carbon future: (i) a reference scenario based on energy and fuel projections of the International Energy Agency (IEA) (*8*) regional and global livestock projections (*9*) and incorporating all presently agreed policies affecting emissions (*10*); (ii) a CH_4 measures scenario that follows the reference but also adds the CH_4 measures; (iii) CH_4+BC measures scenarios that follow the reference but add the CH_4 and one or both sets of BC measures; (iv) a CO_2 measures scenario under which CO_2 emissions follow the IEA's "450 CO_2-equivalent" scenario (*8*) as implemented in the GAINS model (affecting CO_2 and co-emissions of SO_2 but not other long-lived gases); and (v) a combined CO_2 plus CH_4 and BC measures scenario. Measures are phased in linearly from 2010 through 2030, after which only trends in CO_2 emissions are included, with other emissions kept constant.

Emissions from these scenarios were then used with the ECHAM5-HAMMOZ (*11*) and GISS-PUCCINI (*12*) three-dimensional composition-climate models to calculate the impacts on atmospheric concentrations and radiative forcing (*7*). Changes in surface $PM_{2.5}$ (particles of less than 2.5 micrometers) and tropospheric ozone were used with published concentration-response relationships (*13*–*15*) to calculate health and agricultural impacts. CH_4 forcing was calculated from the modeled CH_4 concentrations. Direct ozone and aerosol radiative forcings were produced by using the fraction of total anthropogenic direct radiative forcing removed by the emission control measures, as calculated in the two models, multiplied by the best estimate and uncertainty range for direct forcing, which was determined from a literature assessment. Albedo forcing was similarly estimated on the basis of the fractional decrease of BC deposition to snow and ice surfaces. Indirect and semidirect forcings were estimated by simply assuming that these had the same fractional changes as the direct forcings (*16*). Initially, analytic equations representing rapid and slow components of the climate system

[1]NASA Goddard Institute for Space Studies and Columbia Earth Institute, Columbia University, New York, NY 10025, USA. [2]Stockholm Environment Institute, Environment Department, University of York, York YO10 5DD, UK. [3]Joint Research Centre of the European Commission, Ispra 21027, Italy. [4]International Institute for Applied Systems Analysis, Laxenburg A-2361, Austria. [5]U.S. Environmental Protection Agency, Washington, DC 20460, USA. [6]Department of Economics, Middlebury College, Middlebury, VT 05753, USA. [7]Department of Environmental Health, Harvard School of Public Health, Boston, MA 02215, USA. [8]Argonne National Laboratory, Argonne, IL 60439, USA. [9]Scripps Institute of Oceanography, University of California, San Diego, San Diego, CA 92093, USA. [10]Asian Institute of Technology, Bangkok 10400, Thailand. [11]Environmental Research Group, King's College London, London SE1 9NH, UK. [12]United Nations Environment Programme (UNEP), Nairobi 00100, Kenya. [13]Center for Ecology and Hydrology, Midlothian EH26 0QB, UK.

*To whom correspondence should be addressed. E-mail: drew.t.shindell@nasa.gov

†Present address: Eurasia Institute of Earth Sciences, Istanbul Technical University, Istanbul 34469, Turkey.

(*17*) were used to estimate global and regional (*18*) mean temperature response to the forcings.

This analytic analysis shows that the measures substantially reduce the global mean temperature increase over the next few decades by reducing tropospheric ozone, CH_4, and BC (Fig. 1). The short atmospheric lifetime of these species allows a rapid climate response to emissions reductions. In contrast, CO_2 has a very long atmospheric lifetime (hence, growing CO_2 emissions will affect climate for centuries), so that the CO_2 emissions reductions analyzed here hardly affect temperatures before 2040. The combination of CH_4 and BC measures along with substantial CO_2 emissions reductions [a 450 parts per million (ppm) scenario] has a high probability of limiting global mean warming to <2°C during the next 60 years, something that neither set of emissions reductions achieves on its own [which is consistent with (*19*)].

Work to this stage was largely in support of the Integrated Assessment of Black Carbon and Tropospheric Ozone (*20*). Here, we present detailed climate modeling and extend impact analyses to the national level, where regulations are generally applied and which provides detailed spatial information that facilitates regional impact analyses. We also provide cost/benefit analyses.

Climate modeling. We performed climate simulations driven by the 2030 CH_4 plus BC measures, by greenhouse gas changes only, and by reference emissions using the GISS-E2-S model; the same GISS atmosphere and composition models were coupled to a mixed-layer ocean (allowing ocean temperatures, but not circulation, to adjust to forcing). Direct, semidirect (aerosol effects on clouds via atmospheric heating), indirect (aerosol effects on clouds via microphysics), and snow/ice albedo (by BC deposition) forcings were calculated internally (*7*). We analyzed the equilibrium response 30 to 50 years after imposition of the measures, which is comparable with the latter decades in the analytic analysis.

The global mean response to the CH_4 plus BC measures was −0.54 ± 0.05°C in the climate model. The analytic equations yielded −0.52°C (−0.21 to −0.80°C) for 2070, which is consistent with these results. Climate model uncertainty only includes internal variations, whereas the analytic estimate includes uncertainties in forcing and climate sensitivity (but has no internal variability).

We also examined individual forcing components. Direct global mean aerosol forcings in the ECHAM and GISS models are almost identical (Table 1), despite large uncertainties generally present in aerosol forcing and the two aerosol models being fundamentally different [for example, internal versus external mixtures (*7*)]. CH_4 and ozone responses to CH_4 emissions changes are also quite similar. Ozone responses to changes in CO, volatile organic compounds, and NO_x associated with the BC measures are quite different, however. This is consistent with the nonlinear response of ozone to these precursors (*21*).

The combined indirect and semidirect radiative forcing by all aerosols in the GISS model is negative for the BC Tech and Reg measures. Although sulfate increases slightly—largely because of increases in the oxidant H_2O_2—in all emissions control scenarios, the BC measures primarily decrease BC and organic carbon (OC). The negative forcing suggests that a decreased positive semidirect effect may outweigh decreased negative indirect effects of BC and OC in this model [studies differ on the magnitude of these effects (*22*–*24*)]. Indirect effects are much larger than net direct effects for the Tech measures.

Global mean BC albedo forcing in the model is very small (Table 1), but we assume its

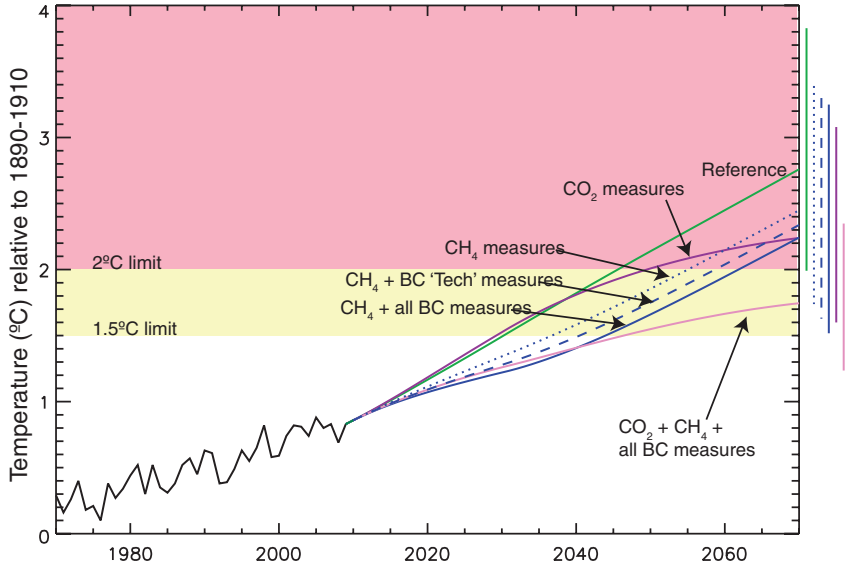

Fig. 1. Observed temperatures (*42*) through 2009 and projected temperatures thereafter under various scenarios, all relative to the 1890–1910 mean. Results for future scenarios are the central values from analytic equations estimating the response to forcings calculated from composition-climate modeling and literature assessments (*7*). The rightmost bars give 2070 ranges, including uncertainty in radiative forcing and climate sensitivity. A portion of the uncertainty is systematic, so that overlapping ranges do not mean there is no significant difference (for example, if climate sensitivity is large, it is large regardless of the scenario, so all temperatures would be toward the high end of their ranges; see www.giss.nasa.gov/staff/dshindell/Sci2012).

Table 1. ECHAM and GISS forcing (W/m^2) at 2030 due to the measures relative to the reference. Dashes indicate forcing not calculated.

	CH_4 measures	CH_4+BC Tech measures	All measures
ECHAM ozone	−0.09	−0.10	−0.10
GISS ozone	−0.10	−0.17	−0.19
ECHAM direct aerosols*	−0.01	−0.06	−0.15
GISS direct aerosols*	−0.01	−0.06	−0.17
(BC, OC, sulfate, nitrate)	(0.00, 0.00, −0.02, 0.00)	(-0.10, 0.06, −0.02, 0.01)	(−0.22, 0.07, −0.02, 0.01)
ECHAM CH_4†	−0.22	−0.22	−0.20
GISS CH_4†	−0.20	−0.20	−0.18
GISS indirect and semidirect aerosols	—	−0.14 ± 0.03	−0.16 ± 0.04
GISS BC albedo (effective forcing ×5)	—	−0.010 (−0.05)	−0.017 (−0.09)
GISS net‡	−0.32	−0.60	−0.77

*For aerosols, the value for ECHAM is the sum of the direct BC+OC+sulfate forcing. For GISS, the same sum is presented first, and individual components are listed afterward (the ECHAM model has more realistic internally mixed aerosols, so components are not separable). †CH_4 forcing at 2030 is roughly 75% of the forcing that is eventually realized from CH_4 emission changes through 2030. ‡The net forcing given here includes the effective value for BC albedo forcing. Uncertainties due to internal variability in the models are 0.01 W/m^2 or less for direct forcings and 0.001 W/m^2 for BC albedo forcing.

"effective" forcing is five times the instantaneous value (*25*, *26*). Albedo forcing can be important regionally (Fig. 2), especially in the Arctic and the Himalayas, where the measures decrease forcing up to 4 W/m^2 (not including the factor of 5). Such large regional impacts are consistent with other recent studies (*27*, *28*) and would reduce snow and ice melting.

Roughly half the forcing is relatively evenly distributed (from the CH_4 measures). The other half is highly inhomogeneous, especially the strong BC forcing, which is greatest over bright desert and snow or ice surfaces. Those areas often exhibit the largest warming mitigation, making the regional temperature response to aerosols and ozone quite distinct from the more homogeneous response to well-mixed greenhouse gases (Fig. 2) [although the impact of localized forcing extends well beyond the forcing location (*29*)]. BC albedo and direct forcings are large in the Himalayas, where there is an especially pronounced response in the Karakoram, and in the Arctic, where the measures reduce projected warming over the next three decades by approximately two thirds and where regional temperature response patterns correspond fairly closely to albedo forcing (for example, they are larger over the Canadian archipelago than the interior and larger over Russia than Scandinavia or the North Atlantic).

The largest precipitation responses to the CH_4 plus BC measures are seen in South Asia, West Africa, and Europe (Fig. 2). The BC measures greatly reduce atmospheric forcing—defined as top-of-the-atmosphere minus surface forcing—in those parts of Asia and Africa (fig. S4), which can strongly influence regional precipitation patterns (*30*–*32*). In comparison with a semiempirical estimate (*33*), the two composition-climate models represent present-day atmospheric forcing reasonably well (fig. S4). The response to greenhouse gases alone shows different spatial structure over South Asia and Europe and is much weaker everywhere (per unit of global mean forcing). The BC measures moderate a shift in the monsoon westward away from Southeast Asia into India seen during 20th- and 21st-century GISS-E2 simulations, with especially strong impacts at the Indian west coast and from Bengal to the northwest along the Himalayan foothills. Climate models' simulations of monsoon responses to absorbing aerosols vary considerably (*30*–*32*). The results suggest that the BC measures could reduce drought risk in Southern Europe and the

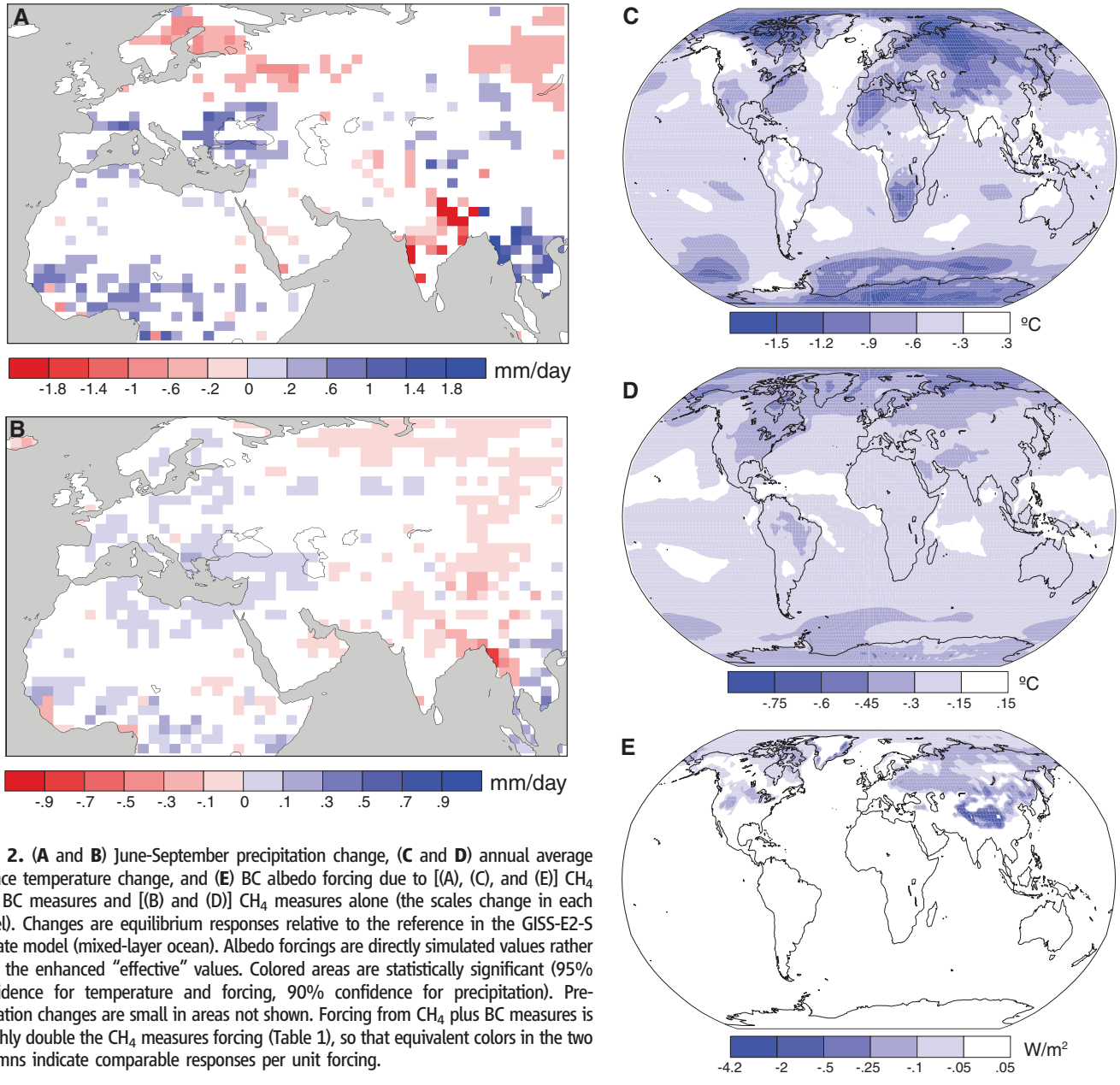

Fig. 2. (**A** and **B**) June-September precipitation change, (**C** and **D**) annual average surface temperature change, and (**E**) BC albedo forcing due to [(A), (C), and (E)] CH_4 plus BC measures and [(B) and (D)] CH_4 measures alone (the scales change in each panel). Changes are equilibrium responses relative to the reference in the GISS-E2-S climate model (mixed-layer ocean). Albedo forcings are directly simulated values rather than the enhanced "effective" values. Colored areas are statistically significant (95% confidence for temperature and forcing, 90% confidence for precipitation). Precipitation changes are small in areas not shown. Forcing from CH_4 plus BC measures is roughly double the CH_4 measures forcing (Table 1), so that equivalent colors in the two columns indicate comparable responses per unit forcing.

Sahel while reversing shifting monsoon patterns in South Asia.

Global mean impacts of packages of measures. Having established the credibility of the analytic climate calculations at the global scale [air quality simulations were shown to be realistic in (*20*)], we now briefly compare the global effects of the separate packages of measures (Table 2). The CH_4 measures contribute more than half the estimated warming mitigation and have the smallest relative uncertainty. BC Tech measures have a larger climate impact and a substantially smaller fractional uncertainty than that of the Reg measures because aerosols contribute a larger portion of the total forcing in the Reg case (and uncertainty in radiative forcing by BC or OC is much larger than for CH_4 or ozone). In the Reg case, the temperature range even includes the possibility of weak global warming, although the distribution shows a much larger probability of cooling.

For yield losses of four staple crops due to ozone, the mean values for CH_4 and BC Tech measures are comparable, whereas BC Reg measures have minimal impact. The health benefits from BC measures are far larger that those from the CH_4 measures because health is more sensitive to reduced exposure to $PM_{2.5}$ than to ground-level ozone. The large ranges for health impacts stem primarily from uncertainty in concentration-response relationships. The estimated 0.7 to 4.7 million annually avoided premature deaths are substantial in comparison with other causes of premature death projected for 2030, including tuberculosis (0.6 million), traffic accidents (2.1 million), or tobacco use (8.3 million) (*34*). There would also be large health benefits from improved indoor air quality. Because of limited data, we only estimated these for India and China, where implementation of all BC measures leads to an additional 373,000 annually avoided premature deaths (*7*).

Cost and benefit valuation. Economic analyses use the value of a statistical life (VSL) for health, world market prices for crops, and the social cost of carbon (SCC) along with global mean impacts relative to CO_2 for climate (*7*). Valuation is dominated by health effects and hence by the BC measures (Table 2). Climate valuation is large for the CH_4 measures, although it depends strongly on the metrics used. If instead of the 100-year GWP, the 100-year global temperature potential (GTP) of CH_4 is used (*35*), the value becomes $159 billion. Similarly, benefits scale with differing choices for the SCC. Climate benefits for the BC measures are based on the CH_4 measures' climate benefits times the relative global mean climate impact of the BC measures because published GWP or GTP values do not cover all species and ignore some factors affecting climate (such as aerosol indirect effects), and the ratio of the temperature responses is similar to the ratio of the integrated forcing due to a single year's emissions (GWP). This method still neglects regional effects of these pollutants on temperatures, precipitation, and sunlight available for photosynthesis.

Because the CH_4 measures largely influence CH_4 emissions alone, and CH_4 emissions anywhere have equal impact, it is straightforward to value CH_4 reductions by the metric ton. Climate benefits dominate, at $2381 per metric ton, with health second and crops third. The climate benefit per metric ton is again highly dependent on metrics. For example, instead of a $265 SCC (*36*)—a typical value assuming a near-zero discount rate—a value of $21 consistent with a ~3% discount rate could be used. Because discounting emphasizes near-term impacts, we believe a 20-year GWP or GTP should be used with the $21 SCC, in which case the valuation is $599 or $430 per metric ton, respectively. Health and agricultural benefits could also be discounted to account for the time dependence of the ozone response. Using a 5% discount rate, the mean health and agricultural benefits decrease relative to the undiscounted Table 2 values to $659 and $18 per metric ton, respectively. Climate benefits always exceed the agricultural benefits per metric ton, but climate values can be less or more than health benefits depending on the metric choices (the health benefits are similarly dependent on the assumed VSL).

A very conservative summation of benefits, using $430 for climate and discounted health and agricultural values, gives a total benefit of ~$1100 per metric ton of CH_4 (~$700 to $5000 per metric ton, using the above analyses). IEA estimates (*37*) indicate roughly 100 Tg/year of CH_4 emissions can be abated at marginal costs below $1100, with more than 50 Tg/year costing less than 1/10 this valuation (including the value of CH_4 captured for resale). Analysis using more recent cost information in the GAINS model (*38*, *39*) finds that the measures analyzed here could reduce 2030 CH_4 emissions by ~110 Tg at marginal costs below $1500 per metric ton, with 90 Tg below $250. The full set of measures reduce emissions by ~140 Tg, indicating that most would produce benefits greater than—and for approximately two-thirds of reductions far greater than—the abatement costs. Of course, the benefits would not necessarily accrue to those incurring costs.

Prior work valued CH_4 reductions at $81 ($48 to $116) per metric ton, including agriculture (grains), forestry, and nonmortality health benefits using 5% discounting (*40*). Their agricultural valuation was ~$30 ($1 to $42) per metric ton. Hence, our agriculture values are smaller but well within their large range. Those results suggest that forestry and nonmortality health effects contribute another ~$50 per metric ton of CH_4. Nonlinearities imply all valuations may shift somewhat as the background atmospheric composition changes.

GAINS estimates show that improved efficiencies lead to a net cost savings for the brick kiln and clean-burning stove BC measures. These account for ~50% of the BC measures' impact. The regulatory measures on high-emitting vehicles and banning of agricultural waste burning, which require primarily political rather than economic investment, account for another 25%. Hence, the bulk of the BC measures could probably be implemented with costs substantially less than the benefits given the large valuation of the health impacts (Table 2).

CH_4 measures by sector and region. It is also straightforward to separate the impact of CH_4 reductions in each region and sector on forcing. Because CH_4 is relatively well mixed globally, other impacts (such as crop yields) have the same proportionality as forcing. Emissions reductions in the coal mining and oil/gas production sectors

Table 2. Global impacts of measures on climate, agriculture, and health and their economic valuation. Valuations are annual values in 2030 and beyond, due to sustained application of the measures, which are nearly equal to the integrated future valuation of a single year's emissions reductions (without discounting). Climate valuations for CH_4 use GWP100 and an SCC of $265 per metric ton (*36*). Crop and health valuations use 95% confidence intervals, whereas climate valuations use ~67% uncertainty range. All values are in 2006 dollars.

	CH_4 measures	BC Tech measures	BC Reg measures
Physical Impacts			
Avoided warming in 2050 (°C)	0.28 ± 0.10	0.12 (+0.06/–0.09)	.07 (+.04/–0.09)
Annually avoided crop yield losses (millions metric tons; sum of wheat, rice, maize, and soy)	27 (+42/–20)	24 (+72/–21)	2 (+13/–3)
Annually avoided premature deaths (thousands)	47 (+40/–34)	1720 (+1529/–1188)	619 (+639/–440)
Valuation			
Climate, billions $US	331 ± 118	142 (+71/–106)	83 (+47/–106)
($US per metric ton CH_4)	(2381 ± 850)		
Crops, billions $US	4.2 ± 1.2	3.6 ± 2.6	0.4 ± 0.6
($US per metric ton CH_4)	(29 ± 8)		
Health, billions $US	148 ± 99	3717 (+3236/–2563)	1425 (+1475/–1015)
($US per metric ton CH_4)	(1080 ± 721)		

have the largest impacts, with municipal waste third (Fig. 3). Globally, sectors encompassing fossil fuel extraction and distribution account for nearly two thirds of the benefits because technology to control emissions from these sectors is readily available.

Examining benefits by sector and region, the largest by a considerable amount are from coal mining in China (Fig. 3). Oil and gas production in Central Africa, the Middle East, and Russia are next, followed by coal mining in South Asia, gas transmission in Russia (in high-pressure mains), and municipal waste in the United States and China. Ranking is obviously quite sensitive to regional groupings and country size, and there is substantial uncertainty in emissions from certain sectors in some regions. In particular, using national emission factors (instead of the Intergovernmental Panel on Climate Change default methodology) would lower the coal-mining potential from India and Southern Africa substantially. Nonetheless, those eight regional/sectoral combinations alone represent 51% of the total impact from all CH_4 measures.

Regional and national impacts. Upon examination of impacts of the CH_4 plus BC measures, avoided warming is greatest in central and northern Asia, southern Africa, and around the Mediterranean (Fig. 4, fig. S5, and table S5). Three of the top four national-level responses are in countries with strong BC albedo forcing (Tajikistan, Kyrgyzstan, and Russia). In contrast, the atmospheric forcing linked to regional hydrologic cycle disruption is reduced most strongly in south Asia and west Africa, where the measures greatly decrease BC emissions. Total numbers of avoided premature deaths are greatest in developing nations in Asia and Africa with large populations and high PM concentrations (and large emissions changes). Turning to per capita impacts, premature deaths are reduced most strongly in countries of south Asia, followed by central Africa, then east and southeast Asia, in a pattern quite similar to the atmospheric forcing impacts.

For crop production, China, India, and the United States, followed by Pakistan and Brazil, realize the greatest total metric tonnage gains. Looking instead at percentage yield changes, impacts are largest in the Middle East, with large changes also in central and south Asia. There is a large impact on percentage crop yields in Mexico that is quite distinct from neighboring countries, reflecting the influence of local emission changes. Impacts vary greatly between crops for changes in total production (fig. S6), with largest impacts occurring where the distribution and seasonal timing of crop production coincide with high ozone concentrations (*7*). Percentage yield changes are more consistent, however. Additional crop yield benefits would result from the avoided climate change, but they are not considered here.

Avoided warming is spread much more evenly over the Earth than other impacts. Both climate benefits in terms of reductions in regional atmospheric forcing and air quality–related human health benefits are typically largest in the countries of south Asia and central Africa, whereas agricultural benefits are greatest in the Middle East, where ozone reductions are large. Because many nations in these areas face great development challenges, realization of these benefits would be especially valuable in those areas.

Discussion. The results clearly demonstrate that only a small fraction of air quality measures provide substantial warming mitigation. Nonetheless, the CH_4 and BC emissions reduction measures examined here would have large benefits to global and regional climate, as well as to human health and agriculture. The CH_4 measures lead to large global climate and agriculture benefits and relatively small human health benefits, all with high confidence and worldwide distribution. The BC measures are likely to provide substantial global climate benefits, but uncertainties are much larger. However, the BC measures cause large regional human health benefits, as well as reduce regional hydrology cycle disruptions and cryosphere melting in both the Arctic and the Himalayas and improve regional agricultural yields. These benefits are more certain and are typically greatest in and near areas where emissions are reduced. Results are robust across the two composition-climate models. Protecting public health and food supplies may take precedence over avoiding climate change in most countries, but knowing that these measures also mitigate climate change may help motivate policies to put them into practice.

We emphasize that the CH_4 and BC measures are both distinct from and complementary to CO_2 measures. Analysis of delayed implemen-

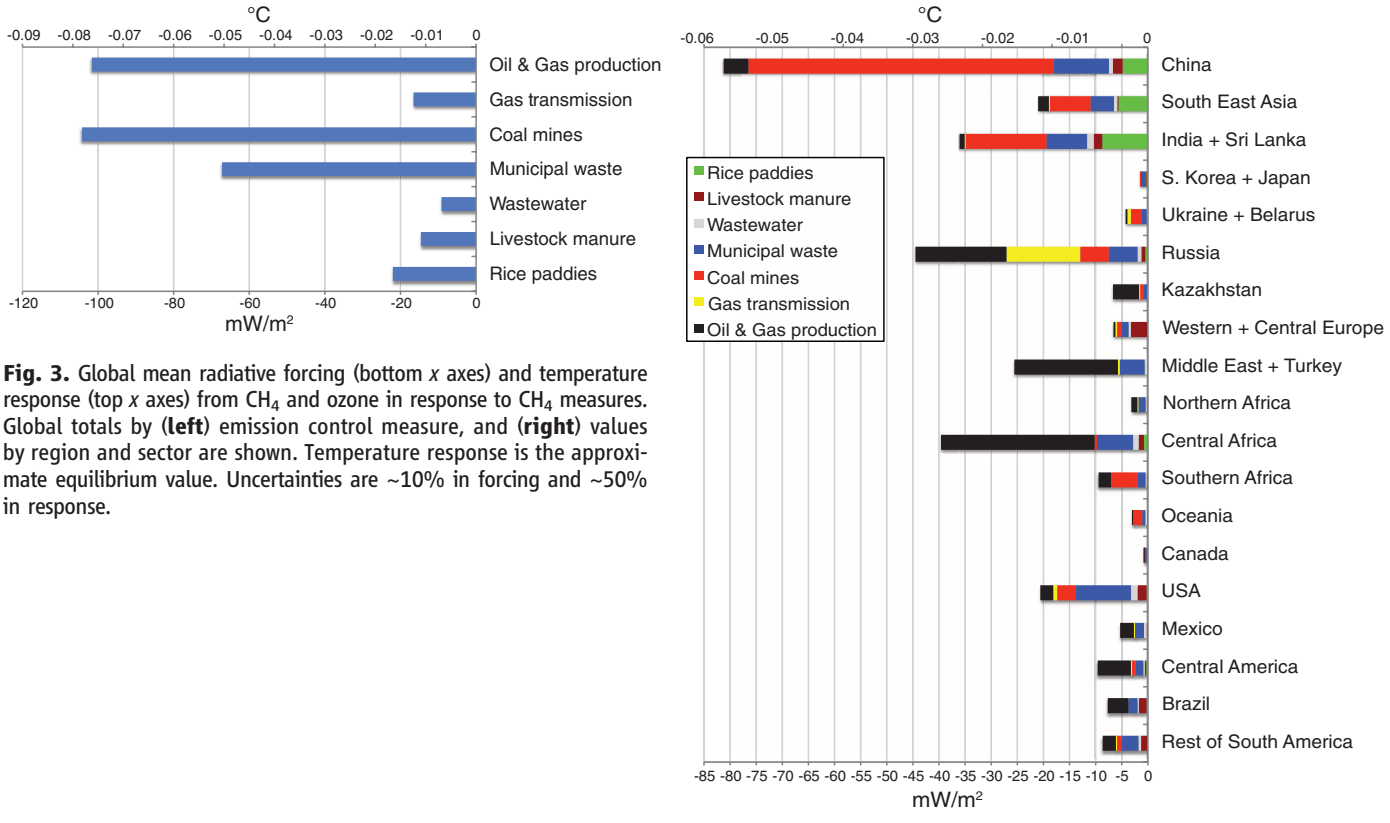

Fig. 3. Global mean radiative forcing (bottom *x* axes) and temperature response (top *x* axes) from CH_4 and ozone in response to CH_4 measures. Global totals by (**left**) emission control measure, and (**right**) values by region and sector are shown. Temperature response is the approximate equilibrium value. Uncertainties are ~10% in forcing and ~50% in response.

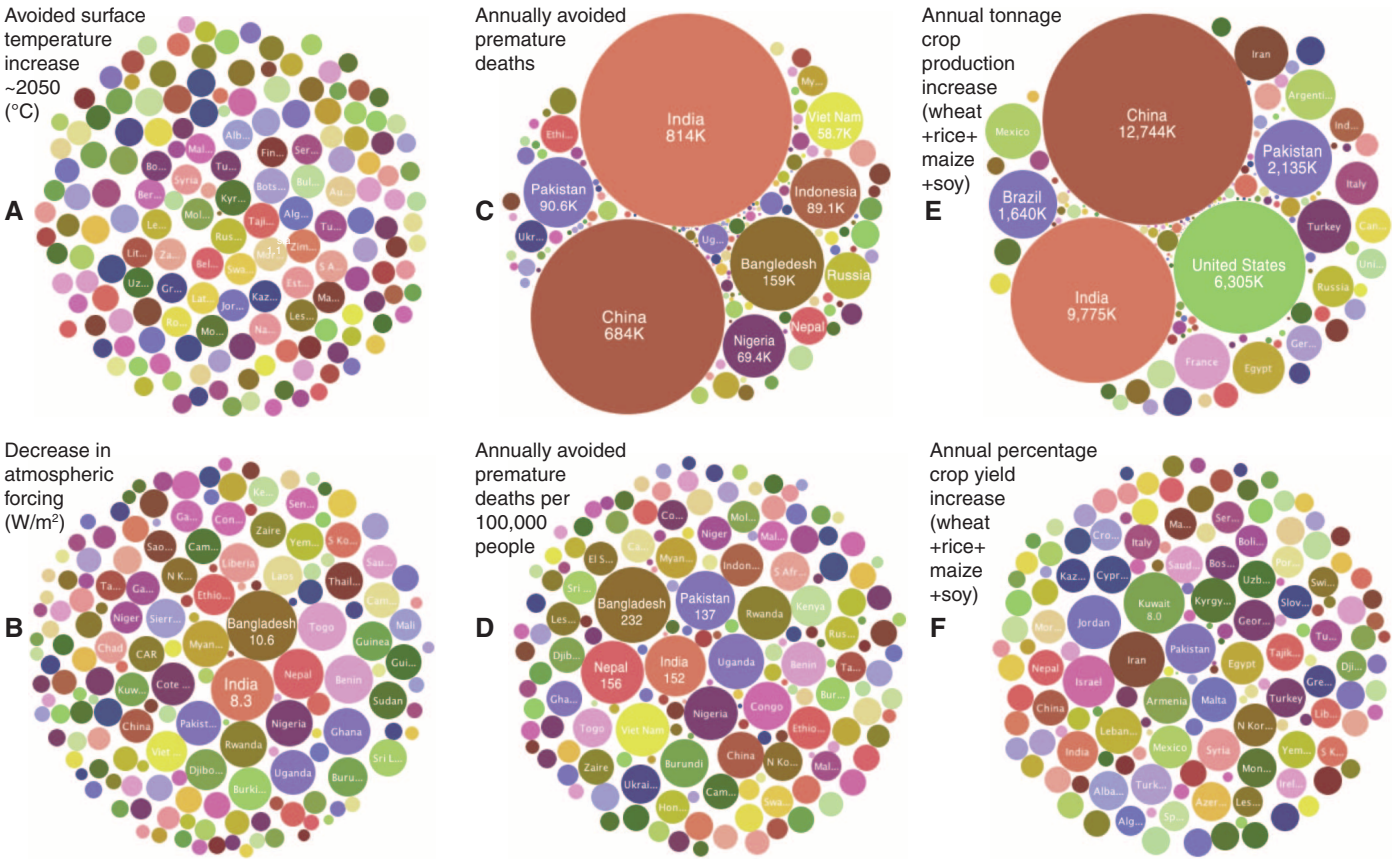

Fig. 4. National benefits of the CH_4 plus BC measures versus the reference scenario. Circle areas are proportional to values for (**A** and **B**) climate change, (**C** and **D**) human health (values for population over age 30), and (**E** and **F**) agriculture. Surface temperature changes are from the GISS-E2-S simulation. Health, agriculture, and atmospheric forcing impacts are based on the average of GISS and ECHAM concentration changes and are for 2030 and beyond. Uncertainties are ~60% for global mean temperatures, with national scale uncertainties likely greater, ~60% for atmospheric forcing, ~70% for health, and roughly −70%/+100% for crops [see (*7*) for factors included in uncertainties, most of which are systematic for atmospheric forcing, health, and agriculture so that much smaller differences between regions are still significant]. Interactive versions providing values for each country are at www.giss.nasa.gov/staff/dshindell/Sci2012, whereas alternate presentations of these data are in fig. S5 and table S5.

tation of the CH_4 and BC measures (fig. S3) shows that early adoption provides much larger near-term benefits but has little impact on long-term temperatures (*20*). Hence, eventual peak warming depends primarily on CO_2 emissions, assuming air quality–related pollutants are removed at some point before peak warming.

Valuation of worldwide health and ecosystem impacts of CH_4 abatement is independent of where the CH_4 is emitted and usually outweighs abatement costs. These benefits are therefore potentially suitable for inclusion in international mechanisms to reduce CH_4 emissions, such as the Clean Development Mechanism under the United Nations Framework Convention on Climate Change or the Prototype Methane Financing Facility (*41*). Many other policy alternatives exist to implement the CH_4 and BC measures, including enhancement of current air quality regulations. The realization that these measures can slow the rate of climate change and help keep global warming below 2°C relative to preindustrial in the near term, provide enhanced warming mitigation in the Arctic and the Himalayas, and reduce regional disruptions to traditional rainfall patterns—in addition to their local health and local-to-global agricultural benefits—may help prompt widespread and early implementation so as to realize these manifold benefits.

References and Notes

1. M. Z. Jacobson, *J. Geophys. Res.* **115** (D14), D14209 (2010).
2. D. T. Shindell *et al.*, *J. Geophys. Res.* **111**, D08302 (2006).
3. P. Forster *et al.*, in *Climate Change 2007: The Physical Science Basis*, S. Solomon, Ed. (Cambridge Univ. Press, New York, 2007).
4. P. Stier, J. Feichter, E. Roeckner, S. Kloster, M. Esch, *Atmos. Chem. Phys.* **6**, 3059 (2006).
5. Z. Klimont *et al.*, *Tellus B Chem. Phys. Meterol.* **61**, 602 (2009).
6. K. Kupiainen, Z. Klimont, *Atmos. Environ.* **41**, 2156 (2007).
7. Materials and methods are available as supporting material on *Science* Online.
8. International Energy Agency, *World Energy Outlook* (OECD/IEA, Paris, 2009).
9. N. Alexandratos *et al.*, "World agriculture: Towards 2030/2050. Interim report. Prospects for food, nutrition, agriculture and major commodity groups" (Food and Agriculture Organization, Rome, 2006).
10. J. Cofala, M. Amann, Z. Klimont, K. Kupiainen, L. Hoglund-Isaksson, *Atmos. Environ.* **41**, 8486 (2007).
11. L. Pozzoli *et al.*, *J. Geophys. Res.* **113** (D7), D07308 (2008).
12. D. T. Shindell *et al.*, *Atmos. Chem. Phys.* **6**, 4427 (2006).
13. D. Krewski *et al.*, "Extended follow-up and spatial analysis of the American Cancer Society study linking particulate air pollution and mortality" (Health Effects Institute, Boston, 2009).
14. M. Jerrett *et al.*, *N. Engl. J. Med.* **360**, 1085 (2009).
15. R. Van Dingenen *et al.*, *Atmos. Environ.* **43**, 604 (2009).
16. V. Ramaswamy *et al.*, in *Climate Change 2001*, J. T. Houghton, Ed. (Cambridge Univ. Press, Cambridge, 2001), pp. 349–416.
17. O. Boucher, P. Friedlingstein, B. Collins, K. P. Shine, *Environ. Res. Lett.* **4**, 044007 (2009).
18. D. Shindell, G. Faluvegi, *Atmos. Chem. Phys.* **10**, 3247 (2010).
19. V. Ramanathan, Y. Xu, *Proc. Natl. Acad. Sci. U.S.A.* **107**, 8055 (2010).
20. United Nations Environment Programme and World Meteorological Organization, "Integrated Assessment of Black Carbon and Tropospheric Ozone" (Nairobi, 2011).
21. S. Sillman, *Atmos. Environ.* **33**, 1821 (1999).
22. D. Koch, A. Del Genio, *Atmos. Chem. Phys.* **10**, 7685 (2010).
23. S. E. Bauer, S. Menon, D. Koch, T. C. Bond, K. Tsigaridis, *Atmos. Chem. Phys.* **10**, 7439 (2010).
24. W. T. Chen, Y. H. Lee, P. J. Adams, A. Nenes, J. H. Seinfeld, *Geophys. Res. Lett.* **37**, L09801 (2010).
25. M. G. Flanner, C. S. Zender, J. T. Randerson, P. J. Rasch, *J. Geophys. Res.* **112** (D11), D11202 (2007).
26. D. Koch *et al.*, *J. Clim.* **22**, 2659 (2009).

27. Y. Qian, M. G. Flanner, L. R. Leung, W. Wang, *Atmos. Chem. Phys.* **11**, 1929 (2011).
28. M. Kopacz *et al.*, *Atmos. Chem. Phys.* **11**, 2837 (2011).
29. D. Shindell *et al.*, *J. Geophys. Res.* **115**, D19110 (2010).
30. G. A. Meehl, J. M. Arblaster, W. D. Collins, *J. Clim.* **21**, 2869 (2008).
31. C. Wang, D. Kim, A. M. L. Ekman, M. C. Barth, P. J. Rasch, *Geophys. Res. Lett.* **36**, L21704 (2009).
32. V. Ramanathan *et al.*, *Proc. Natl. Acad. Sci. U.S.A.* **102**, 5326 (2005).
33. V. Ramanathan, G. Carmichael, *Nat. Geosci.* **1**, 221 (2008).
34. C. D. Mathers, D. Loncar, *PLoS Med.* **3**, e442 (2006).
35. J. S. Fuglestvedt *et al.*, *Atmos. Environ.* **44**, 4648 (2010).
36. R. S. J. Tol, *Economics: The Open-Access, Open-Assessment E-Journal* **2**, 1 (2008).
37. International Energy Agency, "Building the Cost Curves for the Industrial Sources of Non-CO2 Greenhouse Gases" (IEA Greenhouse Gas R&D Programme Cheltenham, UK, 2003).
38. L. Höglund-Isaksson, W. Winiwarter, A. Tohka, "Potentials and costs for mitigation of non-CO2 greenhouse gases in the European Union until 2030—Methodology" (IIASA Report, Laxenburg, Austria, 2010).
39. M. Amann *et al.*, *Environ. Model. Softw.* **26**, 1489 (2011).
40. J. J. West, A. M. Fiore, *Environ. Sci. Technol.* **39**, 4685 (2005).
41. www.globalmethanefund.org; accessed 23 May 2011.
42. J. Hansen *et al.*, *Proc. Natl. Acad. Sci. U.S.A.* **103**, 14288 (2006).

Acknowledgments: Funding was provided by UNEP and the World Meteorological Organization (WMO), NASA's Applied Sciences and Atmospheric Chemistry Modeling and Analysis Programs, and the Clean Air Task Force to IIASA. We thank all the authors and reviewers who contributed to the UNEP/WMO Integrated Assessment of Black Carbon and Tropospheric Ozone.

Supporting Online Material

www.sciencemag.org/cgi/content/full/335/6065/183/DC1
Materials and Methods
Figs. S1 to S6
Tables S1 to S5
References

20 June 2011; accepted 28 November 2011
10.1126/science.1210026

Periodic Emission from the Gamma-Ray Binary 1FGL J1018.6–5856

The Fermi LAT Collaboration*

Gamma-ray binaries are stellar systems containing a neutron star or black hole, with gamma-ray emission produced by an interaction between the components. These systems are rare, even though binary evolution models predict dozens in our Galaxy. A search for gamma-ray binaries with the Fermi Large Area Telescope (LAT) shows that 1FGL J1018.6–5856 exhibits intensity and spectral modulation with a 16.6-day period. We identified a variable x-ray counterpart, which shows a sharp maximum coinciding with maximum gamma-ray emission, as well as an O6V((f)) star optical counterpart and a radio counterpart that is also apparently modulated on the orbital period. 1FGL J1018.6–5856 is thus a gamma-ray binary, and its detection suggests the presence of other fainter binaries in the Galaxy.

Two types of interacting binaries containing compact objects are expected to emit gamma rays (*1*): microquasars—accreting black holes or neutron stars with relativistic jets (*2*)—and rotation-powered pulsars interacting with the wind of a binary companion (*3*). Microquasars should typically be powerful x-ray sources when active, and hence such gamma ray–emitting systems may already be known x-ray binaries. Indeed, the bright x-ray source Cygnus X-3 is now known to be such a source (*4*, *5*). The existence of pulsars interacting with stellar companions of early spectral types is predicted as an initial stage in the formation of high-mass x-ray binaries (HMXBs) containing neutron stars (*6*). These interacting pulsars are predicted to be much weaker x-ray emitters and may not yet be known or classified x-ray sources. Gamma-ray binaries may thus not be as rare as they appear to be, and many systems may await detection.

A gamma-ray binary is expected to show orbitally modulated gamma-ray emission due to a combination of effects, including changes in viewing angle and, in eccentric orbits, the degree of the binary interaction, both of which depend on binary phase. Periodic gamma-ray modulation has indeed been seen in LS 5039 (period 3.9 days), LS I +61° 303 (26.5 days), and Cygnus X-3 (4.8 hours) (*4*, *7*, *8*), and gamma-ray emission is at least orbital phase–dependent for the PSR B1259–63 system (3.4 years) (*9*). However, the putative gamma-ray binary HESS J0632+057, for which a 321-day x-ray period is seen, has not yet been shown to exhibit periodic gamma-ray emission (*10*). PSR B1259–63 contains a pulsar, and LS 5039 and LS I +61° 303 are suspected, but not proved, to contain pulsars, whereas Cygnus X-3 is a black hole candidate. A search for periodic modulation of gamma-ray flux from LAT sources may thus lead to the detection of further gamma-ray binaries, potentially revealing the predicted HMXB precursor population. The first Fermi LAT (*11*) catalog of gamma-ray sources ("1FGL") contains 1451 sources (*12*), a large fraction of which do not have confirmed counterparts at other wavelengths and thus are potentially gamma-ray binaries.

To search for modulation, we used a weighted photon method to generate light curves for all 1FGL sources in the energy range 0.1 to 200 GeV (*13*). We then calculated power spectra for all sources. From an examination of these, in addition to modulation from the known binaries LS I +61° 303 and LS 5039, we noted the presence of a strong signal near a period of 16.6 days from 1FGL J1018.6–5856 (Fig. 1). 1FGL J1018.6–5856 has a cataloged 1- to 100-GeV flux of 2.9×10^{-8} photons cm^{-2} s^{-1}, making it one of the brighter LAT sources. The source's location at right ascension (R.A.) = 10^h 18.7^m, declination (decl.) = –58° 56.30′ (J2000; ±1.8′, 95% uncertainty) means that it lies close to the galactic plane (b = –1.7°), marking it as a good candidate for a binary system. 1FGL J1018.6–5856 has been noted to be positionally coincident with the supernova remnant G284.3–1.8 (*12*) and the TeV source HESS J1018–589 (*14*), although it has not been shown that these sources are actually related.

The modulation at a period of 16.6 days has a power more than 25 times the mean value of the power spectrum and has a false-alarm probability of 3×10^{-8}, taking into account the number of statistically independent frequency bins. From both the power spectrum itself (*15*) and from fitting the light curve, we derived a period of 16.58 ± 0.02 days. The folded light curve (Fig. 1) has a sharp peak together with additional broader modulation. We modeled this to determine the epoch of maximum flux T_{max} by fitting a function consisting of the sum of a sine wave and a Gaussian function, and obtained T_{max} = modified Julian date (MJD) 55403.3 ± 0.4.

The gamma-ray spectrum of 1FGL J1018.6–5856 shows substantial curvature through the LAT passband. To facilitate discussion of the lower-energy (<1 GeV) and higher-energy (>1 GeV) gamma rays, we adopted as our primary model a broken power law with photon indices $\Gamma_{0.1-1}$ and Γ_{1-10} for energies below and above 1 GeV, respectively. The best-fit values (*13*) are $\Gamma_{0.1-1} = 2.00 \pm 0.04_{stat} \pm 0.08_{syst}$ and $\Gamma_{1-10} = 3.09 \pm 0.06_{stat} \pm 0.12_{syst}$, along with an integral energy flux above 100 MeV of $(2.8 \pm 0.1_{stat} \pm 0.3_{syst}) \times 10^{-10}$ erg cm^{-2} s^{-1}. A power law with exponential cutoff (*7*, *8*), $dN/dE = N_0(E/\mathrm{GeV})^{-\Gamma} \exp(-E/E_c)$, gives an acceptable fit with $\Gamma = 1.9 \pm 0.1$ and $E_c = 2.5 \pm 0.3$ GeV (statistical errors only). Although this spectral shape is qualitatively similar to that of pulsars and of LS I +61° 303 and LS 5039, so far no detection of pulsed gamma-ray emission has been reported (*16*).

To investigate variability on the 16.6-day period, we folded the data into 10 uniform bins in orbital phase and then refit the broken power-law parameters within each phase bin. The resulting

*All authors with their affiliations appear at the end of this paper.